Journal of Biomedical Optics

BiomedicalOptics.SPIEDigitalLibrary.org

Optical coherence tomography in gastroenterology: a review and future outlook

Tsung-Han Tsai
Cadman L. Leggett
Arvind J. Trindade
Amrita Sethi
Anne-Fré Swager
Virendra Joshi
Jacques J. Bergman
Hiroshi Mashimo
Norman S. Nishioka
Eman Namati

SPIE.

Tsung-Han Tsai, Cadman L. Leggett, Arvind J. Trindade, Amrita Sethi, Anne-Fré Swager, Virendra Joshi, Jacques J. Bergman, Hiroshi Mashimo, Norman S. Nishioka, Eman Namati, "Optical coherence tomography in gastroenterology: a review and future outlook," *J. Biomed. Opt.* **22**(12), 121716 (2017), doi: 10.1117/1.JBO.22.12.121716.

Journal of Biomedical Optics 22(12), 121716 (December 2017)

REVIEW

Optical coherence tomography in gastroenterology: a review and future outlook

Tsung-Han Tsai,[a,*] Cadman L. Leggett,[b] Arvind J. Trindade,[c] Amrita Sethi,[d] Anne-Fré Swager,[e] Virendra Joshi,[f] Jacques J. Bergman,[g] Hiroshi Mashimo,[h] Norman S. Nishioka,[i] and Eman Namati[a]
[a]NinePoint Medical, Inc., Bedford, Massachusetts, United States
[b]Mayo Clinics, Division of Gastroenterology and Hepatology, Rochester, Minnesota, United States
[c]North Shore University Hospital and Hofstra Northwell School of Medicine, Division of Gastroenterology, Manhasset, New York, United States
[d]Columbia University Medical Center, Department of Gastroenterology, New York City, New York, United States
[e]Spaarne Gasthuis and Free University Medical Center, Amsterdam, The Netherlands
[f]Ochsner Clinic Foundation, Department of Gastroenterology, New Orleans, Louisiana, United States
[g]Academic Medical Center, Department of Gastroenterology and Hepatology, Amsterdam, The Netherlands
[h]Veterans Affairs Boston Healthcare System and Harvard Medical School, Department of Gastroenterology, Boston, Massachusetts, United States
[i]Massachusetts General Hospital, Gastrointestinal Unit, Boston, Massachusetts, United States

Abstract. Optical coherence tomography (OCT) is an imaging technique optically analogous to ultrasound that can generate depth-resolved images with micrometer-scale resolution. Advances in fiber optics and miniaturized actuation technologies allow OCT imaging of the human body and further expand OCT utilization in applications including but not limited to cardiology and gastroenterology. This review article provides an overview of current OCT development and its clinical utility in the gastrointestinal tract, including disease detection/differentiation and endoscopic therapy guidance, as well as a discussion of its future applications. [DOI: 10.1117/1.JBO.22.12.121716]

Keywords: optical coherence tomography; volumetric laser endomicroscopy; optical biopsy; endoscopic imaging; gastroenterology; Barrett's esophagus; inflammatory bowel disease.

Paper 170591SSRR received Sep. 7, 2017; accepted for publication Dec. 5, 2017; published online Dec. 19, 2017.

1 Introduction to Endoscopic Optical Coherence Tomography

Although great strides have been made with traditional white-light endoscopy (WLE), including high-definition imaging sensors, magnified endoscopy, and most recently enhanced contrast techniques such as narrow band imaging, there still exists a challenge to obtain clinically relevant diagnostic information.[1,2] Since the first publication on optical coherence tomography (OCT) in the early 1990s,[3] development of endoscopic OCT[4] techniques and applications has become a major field of research.[5–8] Recent studies on endoscopic OCT have shown great potential to increase diagnostic accuracy and improve disease management due to its high resolution, volumetric, and subsurface imaging capability. In gastroenterology, research institutes and commercial entities have developed a variety of endoscopic OCT tools to investigate and address issues along the gastrointestinal (GI) tract including the esophagus, stomach, pancreatico-biliary tract, small intestine, and colon. These tools not only provide methods to better understand the pathophysiology of GI diseases but also contribute to the improvement of GI disease management.

1.1 *Optical Coherence Tomography and Fourier-Domain Optical Coherence Tomography*

The working principle of OCT is based on an optical ranging technique known as low coherence interferometry.[9,10] An OCT system can measure the time delay and the signal intensity of the light reflected back from a sample. As opposed to ultrasound where direct detection of this time delay is possible, in OCT the light travels at a speed beyond the capability of electronic detection, and hence an interferometer such as a Michelson interferometer is used. In traditional time-domain OCT (TD-OCT), one arm of the interferometer has a scanning reference path delay that is translated over the designed imaging depth.[11] Each sweep in depth provides a depth profile or A-scan. The second arm of the interferometer typically contains a scanning system that scans the light beam over the sample to collect multiple depth profiles forming a two-dimensional (2-D) image or B-scan. In endoscopic OCT systems, this arm is usually a fiber-optic probe for imaging inside the body. The scanning system and probe determine the field of view, working distance, and the lateral resolution of the imaging system.

In the early 2000s, the introduction of Fourier-domain detection dramatically increased the imaging speed and detection sensitivity of OCT technology.[12–14] While TD-OCT directly measures the interference signal, Fourier-domain OCT measures the spectrum of the interference signal, and the OCT axial scan is obtained by applying a Fourier transform on the detected spectrum without the need for scanning the reference path delay. Fourier-domain OCT can be divided into two implementations, namely spectral-domain OCT (SD-OCT), which measures the spectrum of the interference signal with a spectrometer,[15] and swept source OCT (SS-OCT), also known as optical frequency domain imaging (OFDI), which measures the spectrum of the interference signal with a wavelength-swept light source and a photodetector.[16,17] Due to the availability of existing technology, SS-OCT is typically used for applications requiring fast

*Address all correspondence to: Tsung-Han Tsai, E-mail: TTsai@ninepointmedical.com

imaging speed at wavelengths of 1.3 and 1 μm, while SD-OCT is used for applications requiring high axial resolution from broadband light sources with shorter operating wavelengths.[18,19] Since the first introduction of Fourier-domain OCT in endoscopic systems in 2007,[20,21] SS-OCT at 1.3-μm wavelength has become the predominant technology of choice for endoscopic OCT applications, primarily due to the improved depth penetration in tissue with a longer wavelength source, increased sensitivity of a dual-balanced detection scheme, and the utilization of fiber optics for optical communication.[17,21] To date, advances in wavelength-SSs, data acquisition, and scanning probe technologies have enabled multimegahertz high-speed endoscopic OCT imaging.[22–24]

1.2 *Optical Probes*

As OCT technology continues to mature, imaging probes have become a major development area for endoscopic OCT applications, as they directly interact with patients and determine the optical (lateral resolution, focal depth) and mechanical (scanning speed, sampling density) parameters that are essential for image quality. Previous review publications in the field[25,26] have provided a comprehensive overview and summary of different imaging probe designs and thus we will cover only the probe variants at a high level. There are two major probe configurations as shown in Fig. 1, namely side viewing and forward-viewing probes. Side-viewing probes [Fig. 1(a)] are the most common configuration and used in the majority of endoscopic OCT studies, especially when relatively large image coverage within luminal anatomies is required. Depending on the working distance and lateral resolution requirements of the application, a probe can be packaged in different forms, such as a small diameter flexible sheath,[4] large diameter inflatable balloon,[27] or rigid housing.[28] The scanning mechanism of these probes can be either proximally driven by a motorized fiber optic rotary joint via a drive shaft/torque cable or directly driven by a distal miniaturized scanner, with an additional pullback/push-forward mechanism to achieve three-dimensional (3-D) imaging. The forward viewing probes [Fig. 1(b)], on the other hand, provide a small field of view but offer a more intuitive viewing scheme similar to magnified endoscopy or endomicroscopy. Scanners are typically located distally in the probes and provide 2-D scanning such as raster,[29] spiral,[30] and Lissajou[31] patterns depending on the actuators used in the probe designs. Forward-viewing probes are typically used in applications that require high magnification and integration with other microscopy modalities.

2 Unmet Needs in Gastroenterology and the Benefit of Using Optical Coherence Tomography

Adoption of an advanced imaging technology like endoscopic OCT relies on whether the technology can address issues that cannot be effectively resolved, in terms of both capability and cost, by the current standard of care. It is estimated that 310,440 new GI cancer cases resulting in 157,700 deaths will occur in the United States in 2017.[32] The survival rate from GI cancers can be improved by 5- to 10-fold if diagnosed at an early stage.[32] Current standard procedures to achieve early detection depend on a three-step process: (1) identify a population at risk, (2) perform an endoscopic evaluation to identify a premalignant lesion, and (3) perform tissue retrieval (biopsy or resection) for pathological confirmation. High-definition WLE with magnification and narrow-band imaging can generally identify superficial lesions in the GI tract but small or flat lesions are often subtle and may be missed due to limitations in resolution and light penetration.[33,34] In addition, subsurface malignant or premalignant lesions may not be visible on WLE.

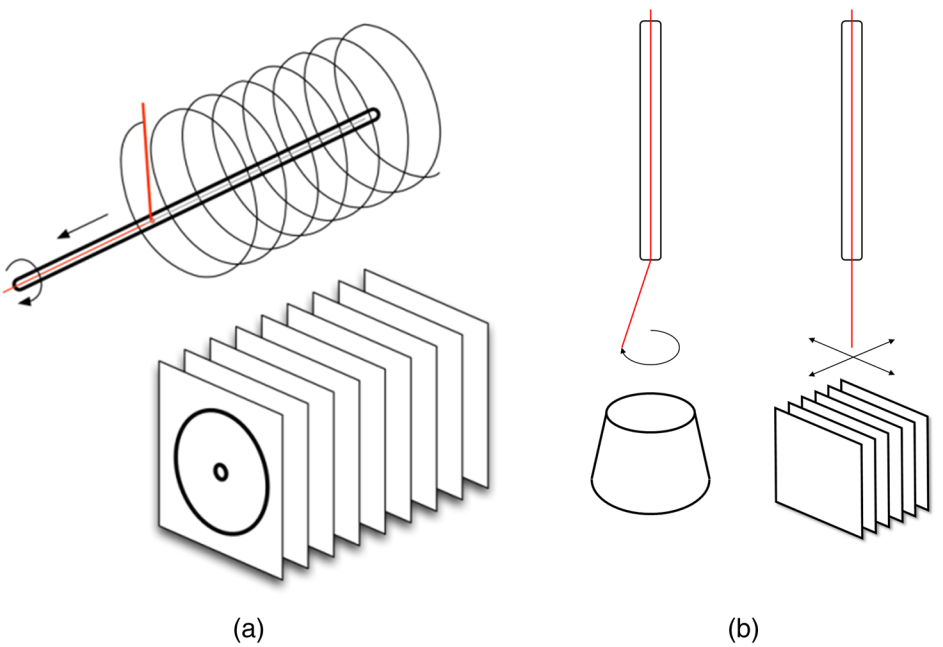

Fig. 1 Endoscopic probe designs and operating principle for OCT imaging: (a) side-viewing configuration rotates the light with longitudinal pullback to generate a series of radial images for three-dimensional reconstructions; (b) forward-viewing configuration scans the light in two-dimensions to achieve volumetric OCT imaging.

The amount of tissue to be sampled is determined by the size and distribution of the premalignant condition. Barrett's esophagus (BE) is the established precursor to esophageal adenocarcinoma. This lesion can extend over several centimeters of the human esophagus and is classified based on its length and distribution. The risk of cancer in BE increases with the degree of dysplasia,[35,36] as the progression of BE to adenocarcinoma is thought to be a stepwise progression from specialized intestinal metaplasia (SIM), low-grade dysplasia (LGD), and high-grade dysplasia (HGD) to intramucosal carcinoma (IMC). Established surveillance protocols for BE recommend targeted biopsies of areas with mucosal abnormalities followed by random four quadrant biopsies at set intervals.[37] However, this approach is limited by sampling error as less than 5% of the total surface area[38] is evaluated. In addition, while dysplasia can manifest with a heterogeneous distribution within a BE segment, suggesting the samples may not truly reflect the degree of dysplasia.[39] Other possible premalignant lesions, such as indeterminate strictures of the biliary tree, are not as easily sampled.[40] An advantage of endoscopic OCT is in providing widefield, subsurface, and near-microscopic imaging to guide targeted tissue retrieval, which may obviate the need to acquire nonsuspicious tissue and improve diagnostic yield.

Endoscopic OCT can also be used as an imaging modality for posttreatment surveillance. GI diseases that are confined to the mucosa can usually be treated with tissue removal techniques such as endoscopic mucosal resection (EMR)[41,42] and endoscopic submucosal dissection,[43] or ablative therapies, such as argon plasma coagulation,[44] radiofrequency ablation (RFA),[45] and cryotherapy.[46,47] The goal of these methods is the same—to remove or destroy the abnormal tissue and allow normal tissue to grow back. Currently, the standard practice for assessment of treatment efficacy is continuous endoscopic surveillance at set intervals.[48] In BE, for example, treated areas typically recover in the form of neosquamous epithelium, which is endoscopically similar to normal squamous epithelium. During treatment, Barrett's glands may become buried under neosquamous epithelium and may elude detection by surveillance biopsies. Although the long-term clinical significance of buried BE is still being studied,[49,50] there are case reports that show an increased risk of malignancy.[51] Endoscopic OCT has several roles in posttreatment surveillance. It can detect buried disease and guide further endoscopic therapy. It can also serve to confirm complete eradication of BE (negative predictive value) and extend follow-up intervals or identify areas of residual disease requiring additional therapy.

3 Endoscopic Optical Coherence Tomography Utilization in the Gastrointestinal Tract

Over the past decade, the majority of endoscopic OCT clinical studies have been performed in the esophagus due to the availability of a commercial system, and comparatively fewer studies have been performed in other areas of the GI tract, such as the stomach, duodenum, bile duct, and colon. This section will describe recent representative studies conducted using the state-of-the-art endoscopic OCT systems for the esophagus as examples of clinical use, followed by a highlight of studies conducted in other areas of the GI tract.

3.1 *Structural Features for Dysplasia Detection in the Esophagus*

As with any new imaging modality, early investigations using OCT were focused on the structural features corresponding to pathology and evaluating the subsurface and high-resolution imaging capabilities. Early studies in the 2000s demonstrated that endoscopic OCT can be used to detect metaplasia in BE patients.[52,53] In a 55-patient study, Evans et al.[54] described structural features including layered architecture, glands, and surface maturation based on OCT image features and developed the criteria to differentiate IMC and HGD from LGD, indeterminate-grade dysplasia (IGD), and SIM with no dysplasia with 83% sensitivity and 75% specificity. This study along with the introduction of high-speed endoscopic balloon-based OCT systems[27] demonstrated the feasibility for clinical esophageal applications and laid down the foundation for commercialization of GI-focused OCT systems. Commercialization enabled broad access to this technology and thereby increased the number of users and patients in both a research and routine clinical setting.

Following the probe-based OCT imaging systems by Imalux Corporation and Lightlab Imaging for general and cardiovascular imaging applications, respectively, the first commercial endoscopic OCT system developed specifically for GI applications was the NvisionVLE® Imaging System, developed by NinePoint Medical™, Inc., now known as volumetric laser endomicroscopy (VLE).[51,55] The system uses a balloon-based imaging probe and can provide real-time volumetric scans from inside the esophagus covering 6 cm length with 7-μm axial resolution and up to 3-mm imaging depth in tissue. Since its launch in 2013, several multicenter and longitudinal clinical studies have been conducted. In 2016 a 1000-patient registry was completed with the participation of 18 major medical centers across the United States[56] and is currently the largest database of esophageal OCT scans along with data evaluating the clinical impact of this technology. Figure 2 includes representative cross-sectional OCT images acquired by NvisionVLE systems with corresponding histology illustrating the structural difference from normal to a variety of pathologies in the esophagus. Leggett et al.[57] established a diagnostic algorithm to detect dysplasia based on the VLE data from 27 patients. This stepwise method allows rating each OCT image based on mucosal layer effacement, presence of atypical glands, and surface-to-subsurface intensity ratio over a 1-cm longitudinal subset of the volumetric dataset. The workflow is shown in Fig. 3 and it is reported that the diagnostic algorithm can achieve 86% sensitivity, 88% specificity, and 87% diagnostic accuracy to detect BE dysplasia with almost perfect interobserver agreement among three raters (kappa = 0.86).[57] A recent independent study conducted by Swager et al.[58] also reported similar VLE features (lack of layering, higher surface signal, and presence of irregular/dilated glands) significantly associated with BE neoplasia. Although these analyses were performed on *ex vivo* EMR samples, the feature-based diagnostic algorithm can serve as a general guideline to help in the interpretation of VLE images and potentially can be adapted *in vivo* with real-time interpretation performed on any regions of interest (ROI) covered by the volumetric data.

According to criteria set by the American Society of Gastrointestinal Endoscopy in the preservation and incorporation of valuable endoscopic innovations criteria for BE,[59] any diagnostic advanced imaging tool must be validated against

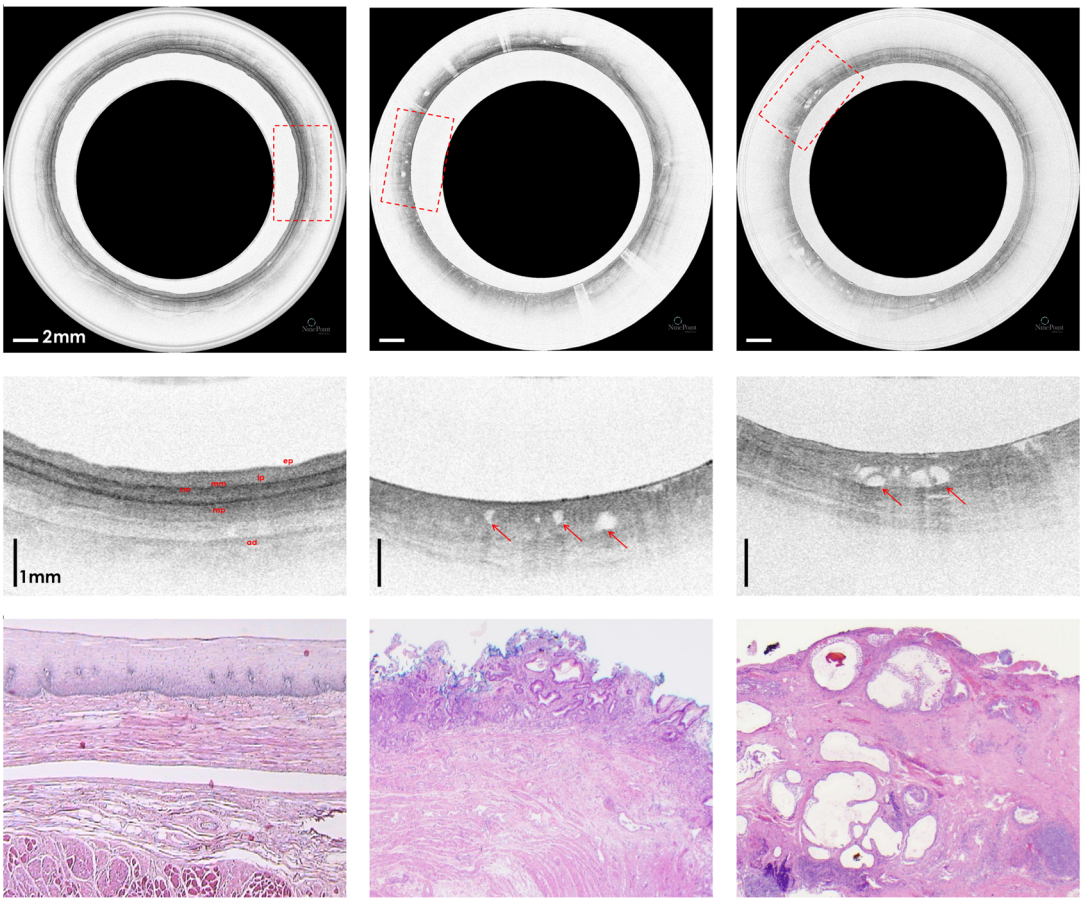

Fig. 2 Representative VLE circumferential (top), magnified (middle), and histological (bottom) images in the esophagus: (a) normal esophagus shows well-defined layered structure; (b) dysplastic BE shows loss of layering and irregular glands; (c) esophageal cancer shows loss of layering with septate cribriform glands. ep, epithelium; lp, lamina propria; mm, muscularis mucosa; sm, submucosa; mp, muscularis propria; ad, adventitia. Arrows indicate irregular glands. Scale bars in VLE images are in tissue. Images provided by NinePoint Medical.

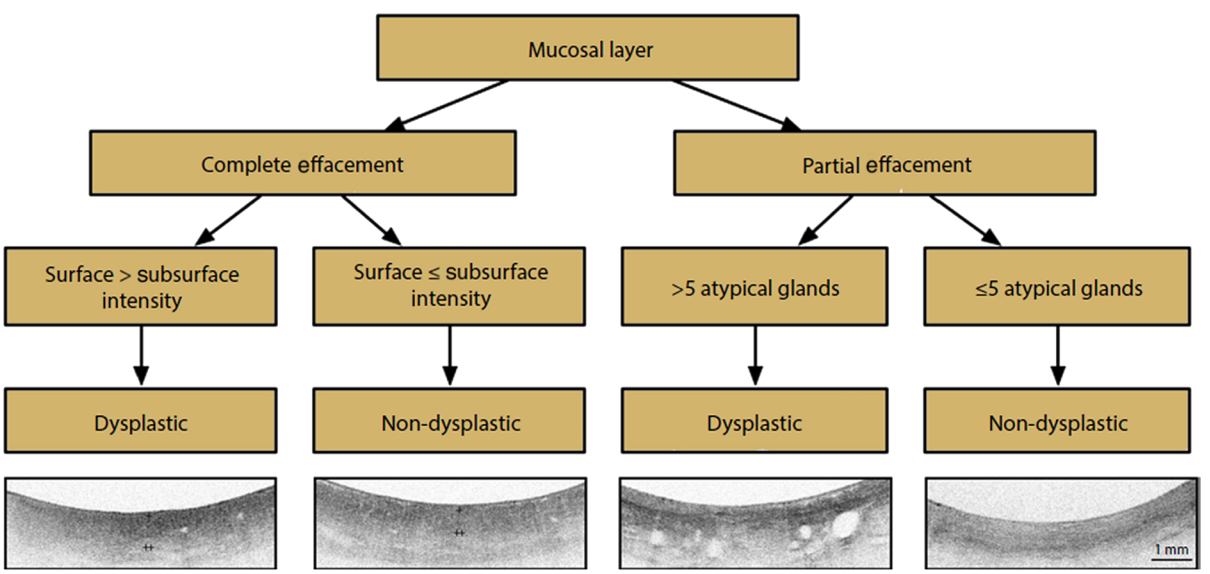

Fig. 3 Flowchart of dysplasia diagnostic algorithm using VLE. The figure is reproduced from Ref. 57.

the histological diagnosis from such imaged locations. In addition the performance of such a tool must meet a per-patient sensitivity >90% and a negative predictive value (NPV) >98% for detecting HGD or early esophageal adenocarcinoma (EAC), as well as a sufficiently high specificity (80%) to allow a reduction of the number of biopsies compared with random biopsies. Early clinical publications that used OCT did not have the ability to provide accurate coregistration among the OCT image, the endoscopic image, and corresponding histology. It is challenging to obtain biopsies from the exact imaged locations because these two activities do not typically happen concurrently even with the use of multichannel endoscopes, especially when the ROI identified from the images are small or not superficial (e.g., a small group of subsurface atypical glands).[60] Researchers have used *in vivo*[50] or *ex vivo*[58] methods to achieve coregistration between OCT images and histology by creating visual landmarks on surrounding tissue. Suter et al.[61] demonstrated an integrated OCT system with the addition of a high-power laser that can create superficial cautery marks around the ROI during real-time OCT imaging. This combined imaging and marking method allowed for precise OCT to histology registration without the need for additional endoscopic tools, thereby allowing seamless integration into the existing clinical workflow.

This laser marking technology was integrated into the second generation of the commercial NvisionVLE system with Real-time Targeting™ and was launched in 2016. The first-in-human study using this system was conducted by Swager et al.[62] In this 16-patient study, the main goal was to evaluate the visibility and locational accuracy of the laser marks made by the system across different tissue types in the esophagus including normal, nondysplastic Barrett's esophagus, LGD, HGD, and early EAC. Figure 4 shows an example of the laser marking workflow, where the VLE balloon probe is deployed at the gastroesophageal junction (GEJ), ROIs are identified and marked with the system, and reidentified under WLE. Overall the visibility of laser marks under WLE was high, with 92% in gastric mucosa, 100% in BE mucosa, and 97% in squamous mucosa.[62] It is also reported that 100% of suspicious regions identified in OCT images were successfully targeted by the laser marks, which allowed biopsy or EMR at the targeted regions. This study demonstrated the feasibility of laser marking-guided biopsy and subsequent tissue retrieval, which can achieve accurate image and tissue coregistration for future OCT clinical studies. More importantly for routine clinical use, this new advancement shows the potential to improve the diagnostic yield and address the major unmet need of current endoscopic practice.

Esophageal squamous cell carcinoma (SCC) is another type of esophageal cancer that has increasing prevalence in Asia.[63] Hatta et al.[64,65] conducted multiple clinical studies with over a hundred patients enrolled and utilized OCT to assess the tumor invasion in superficial SCC. In these studies, the tumor staging criteria were established based on cross-sectional OCT images, and the prospective study reported an overall accuracy of 90.1% with good interobserver agreement ($\kappa = 0.73$) and showed superiority to high-resolution ultrasound for staging SCC.[65] Trindade et al.[66] also published a case report recently that used the NvisionVLE system to stage SCC and consequently guided the physician to select suitable endoscopic therapy. These results highlight the potential of using high-resolution and subsurface imaging capabilities from OCT to guide the assessment and management of esophageal cancer.

3.2 *Endoscopic Therapy Guidance*

In addition to guided biopsy and tissue retrieval, OCT can also be used to guide endoscopic treatment and monitor the treatment efficacy. Researchers at Massachusetts Institute of Technology and VA Boston Healthcare System have conducted a comprehensive series of clinical studies that used endoscopic OCT to evaluate the treatment of BE patients with RFA. It was demonstrated that OCT can be used before the ablation to predict the treatment efficacy based on the BE mucosal thickness,[67] during the ablation to monitor the depth of thermal injury,[68,69] and after the ablation to evaluate tissue recovery and detection of buried glands in follow-up sessions.[70] Although RFA is able to effectively treat dysplasia associated with BE,[45,71,72] a 33% BE recurrence was reported in a multicenter study after 2 years of complete remission of intestinal metaplasia (CRIM) by RFA treatment.[73] There are different hypotheses regarding the cause of BE recurrence, with the presence of buried glands or subsquamous intestinal metaplasia being one of them. Endoscopic OCT can potentially serve as a longitudinal monitoring tool to study the tissue changes over time after treatment. Recently, Swager et al.[50] conducted a 17-patient study using VLE and reported buried Barrett's glands (Fig. 5) in 1 out of 17 patients who had received RFA treatment and achieved CRIM. Significant potential exists for the use of OCT, as it is the only currently available imaging modality for detecting buried disease posttreatment.

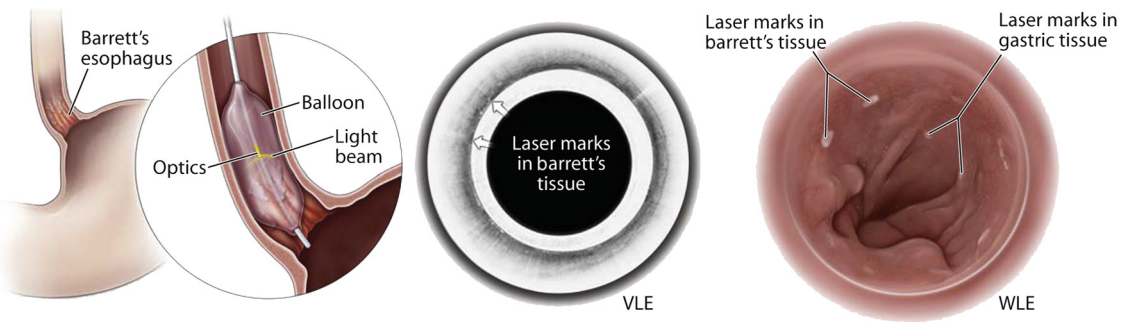

Fig. 4 Integrated real-time laser marking functionality allows coregistration of endoscopic OCT images and histology. The figure is reproduced from Ref. 62.

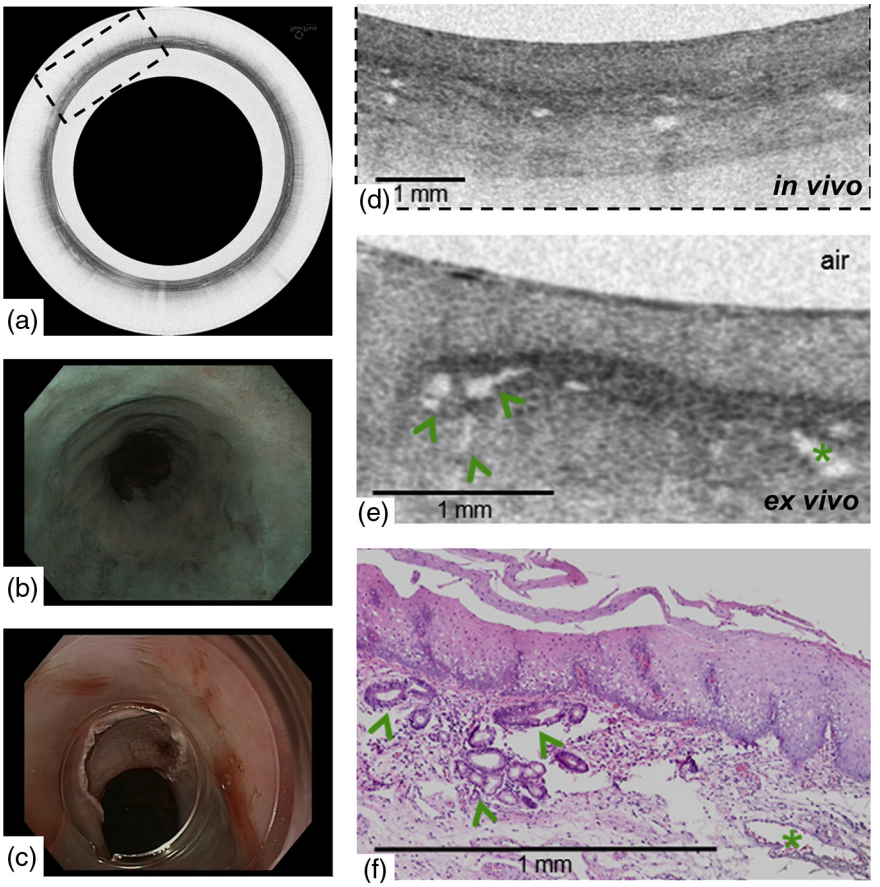

Fig. 5 Endoscopic OCT allows subsurface imaging and is able to detect buried Barrett's glands underneath normal looking esophagus: (a) *in vivo* OCT scan; (b) endoscopic picture with narrow-band imaging showing no residual BE within the neosquamous epithelium; (c) WLE image of the site after endoscopic resection; (d) buried Barrett's glands on the *in vivo* OCT image; (e) buried Barrett's glands on the *ex vivo* OCT image; (f) corresponding histology. Arrowheads indicate buried Barrett's glands and asterisk indicates blood vessel. Originally published in Ref. 50.

3.3 *Barrett's Esophagus Screening Using Optical Coherence Tomography*

The prevalence of BE is estimated to be 5.6% of the general US population[74] with such individuals having a significantly higher risk of developing esophageal adenocarcinoma.[75,76] However, the majority of people with BE are asymptomatic[77] and early detection in the form of a screening test is difficult. The introduction of a tethered OCT capsule in 2013 created significant excitement for endoscopic OCT in the esophagus.[28] The capsule (~12 mm in diameter) allows direct deployment of the optics through swallowing and enables high-resolution circumferential OCT imaging of the esophagus. The fact that it does not require sedation or anesthesia, unlike standard endoscopic procedures, and can provide subsurface structural information makes this technology a promising BE screening tool. This first version performs 2-D cross-sectional imaging and requires longitudinal manipulation from the proximal end to achieve volumetric imaging of the esophagus. To date, this OCT capsule has been used in clinical studies in >100 patients[78,79] with early results demonstrating feasibility, high patient acceptability, and strong potential for clinical impact. With the use of a micromotor and pneumatic translation mechanism, Liang et al.[80,81] developed a capsule probe design (Fig. 6) that enabled precise rotary and longitudinal scanning and demonstrated high speed (250 fps), high-quality volumetric imaging along with *en face* visualization with minimized distortion caused by motion.

The tethered capsule OCT imaging technology in combination with the previously mentioned OCT diagnostic criteria could be used to screen a targeted population and identify patients at highest risk of cancer that would benefit from endoscopic therapy. To gain clinical acceptance, this technology needs to be cost effective, easily operated, and capable of providing quick results.

3.4 *Inflammatory Bowel Disease and Polyps Screening Investigation in Colon*

Outside of the esophagus, the colon is the most studied organ in the GI tract using OCT. Colorectal cancer is the second leading cause of cancer death in the US.[32] Although early detection can be achieved by performing conventional colonoscopy screening, the full polypectomy procedure plus pathology lab process can be time consuming and inefficient in cases with a large number of identified polyps, especially with the majority being hyperplastic polyps. Thus, an imaging modality such as OCT that can provide broad field, subsurface, and near-microscopic imaging capabilities could be used to prescreen the polyps or suspicious regions and help guide treatment.

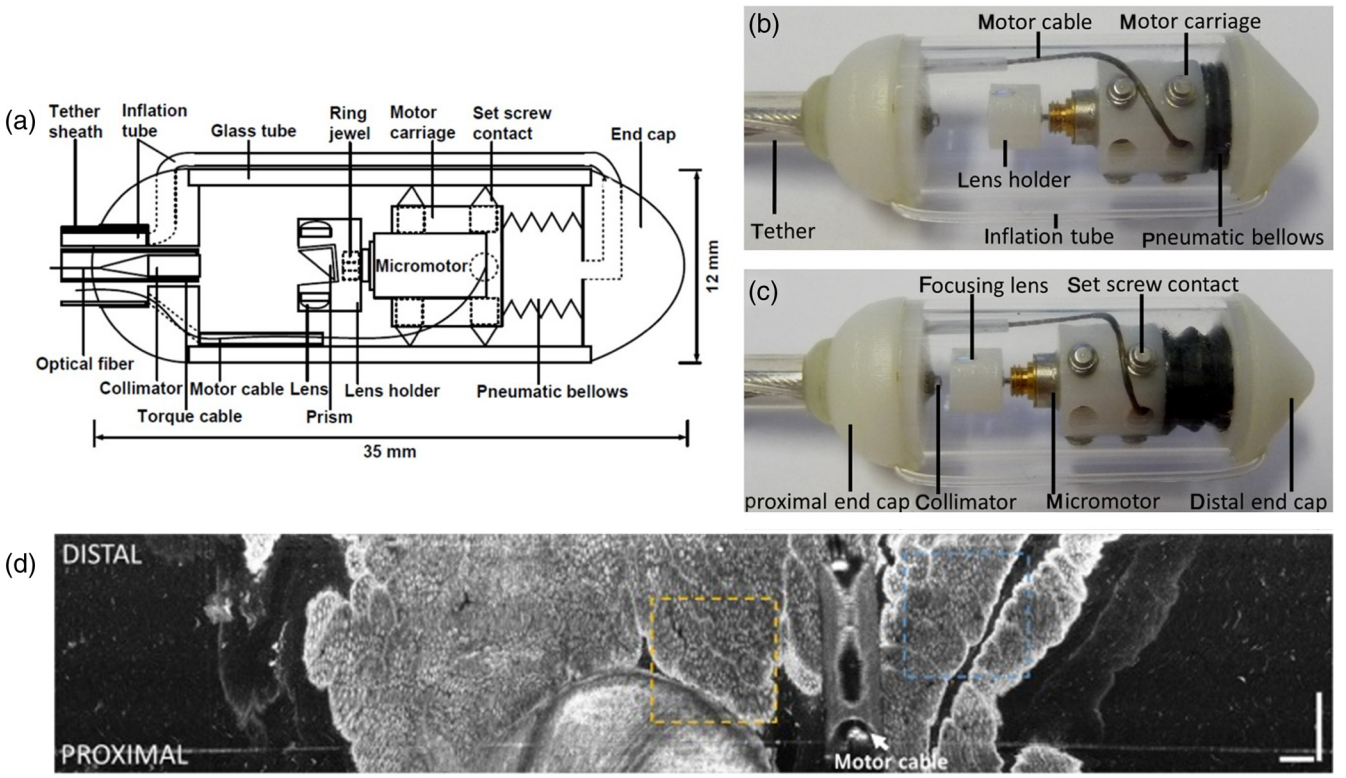

Fig. 6 Tethered capsule with *en face* imaging using pneumatic longitudinal translation: (a) schematic of the device; (b, c) photographs of the device with motor carriage at beginning and ending of longitudinal positions, respectively; (d) *en face* OCT image of swine rectum at 400-μm depth from the surface. Scale bar: 1 mm. Originally published in Ref. 80.

Several *in vivo* studies have been conducted to study the structural difference between colorectal cancer and adenomatous polyps,[82,83] as well as to study the differentiation of inflammatory bowel diseases[84,85] using cross-sectional OCT images. Trindade et al.[86] reported the first case of the NvisionVLE system to evaluate a rectal polyp near the dentate line. Here OCT showed normal submucosa underneath the polyp, which altered the polyp management from full-thickness resection to EMR. The volumetric OCT imaging in the colon also allows visualization of *en face* features for better differentiation of the diseases.[87] Recently, Liang et al.[88] developed a forward-viewing OCT probe using a piezoelectric actuator and demonstrated high-resolution *en face* colon images that are analogous to magnified endoscopic view without requiring contrast agent and providing multidepth visualization. Figure 7 shows *in vivo* volumetric images from a hyperplastic polyp at an imaging speed of 2 volumes per second, which is an encouraging example of *in vivo* polyp assessment using OCT.

3.5 *Visualization of Pancreatico-Biliary Tract Strictures*

Bile duct strictures can be malignant (cholangiocarcinoma) or benign such as those caused by primary sclerosing cholangitis (PSC) and other conditions. Strictures can be challenging to access and to diagnose accurately. Currently, the most common way to differentiate a biliary stricture is to perform endoscopic retrograde cholangiopancreatography (ERCP) with biopsy or brush cytology.[89,90] However, the diagnostic yield is low due to the small tissue sampled and torturous anatomy of the bile duct.[91,92] Researchers have been evaluating endoscopic OCT to help improve the diagnostic accuracy of biliary strictures. With a low-profile OCT probe, such distant and tortuous anatomies can be imaged with high fidelity providing new insights on disease diagnosis and progression. Several preliminary clinical studies have shown that OCT can provide morphological information for biliary strictures, which can be used to differentiate malignant versus benign strictures with high accuracy.[93–95]

The availability of commercialized endoscopic OCT systems has enabled the use of OCT imaging in the evaluation of indeterminate pancreatico-biliary strictures. Tyberg et al.[96] conducted a 9-patient study and demonstrated that strictures with cholangiocarcinoma showed a hyperreflective surface with a loss of inner wall layering while benign biliary strictures showed clear delineated ductal wall layering. Joshi et al.[97] also conducted a 22-patient study that came to similar conclusions, and performed quantification analysis on the thickness of each layer to identify the key features to differentiate benign, inflammatory, and malignant tissue types in the bile duct. Figure 8 shows examples of *in vivo* OCT images in the biliary duct including normal, PSC, and cholangiocarcinoma using the NvisionVLE system with low-profile OCT probes. These studies show that OCT is feasible and has the potential to improve the sensitivity of diagnosing indeterminate strictures.

3.6 *Gastric Lesions Evaluation*

While the majority of OCT studies focused on the esophagus, there are few studies that describe the general structural difference between disease and normal tissue in the stomach. These

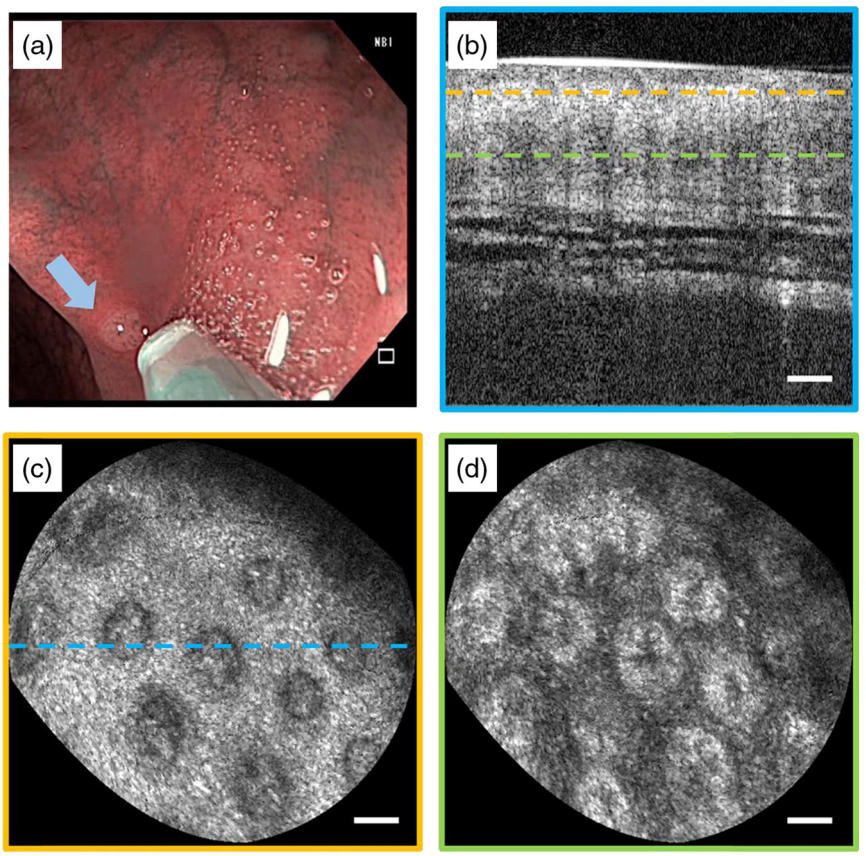

Fig. 7 Forward-viewing probes allow *in situ* polyps assessment during colonoscopy: (a) endoscopic image showing probe in contact with hyperplastic polyp; (b) cross-sectional OCT image from the polyp; (c, d) *en face* OCT visualization of the polyp at 40- and 200-μm depth, respectively, showing enlarged crypts. Scale bars: 100 μm. Originally published in Ref. 88.

include incidental examples that were obtained within GI OCT studies and single case report-based findings that specifically focused on gastric lesions. Recently Xu et al.[98] conducted a 5-patient case study using a commercial NvisionVLE system to identify structural features associated with intestinal metaplasia, LGD, HGD, and submucosal tumor (Fig. 9). Different from the well-defined layered architecture in the esophagus, the cardia has signature "pits and crypts" appearance under OCT cross-sectional images, which potentially can be used as one of the features to differentiate gastric lesions. Using ultrahigh-speed endoscopic OCT with distal motor based scanning probe, Lee et al.[99,100] reported the *en face* OCT findings from patients with gastric antral vascular ectasia (a cause of upper GI bleeding) before and after RFA treatment, which highlighted the potential for OCT to evaluate response to treatment.

3.7 *Disease Research in the Small Intestine*

Compared with the rest of the GI tract, the small intestine is the most challenging anatomy for OCT, or any other endoscopic modality, due to its lengthy and torturous anatomy, and thus the least investigated organ of the GI tract. Most early studies were conducted in the duodenum, the most proximal section of the small intestine, focusing on the detection of celiac disease and Crohn's disease. Celiac disease is an autoimmune disease of the small intestine induced by ingestion of gluten, which leads to the damage of villi ultimately affecting the absorption of nutrients. Since the current standard of care for celiac disease is to confirm a diagnosis pathologically with duodenal biopsies, it also suffers from sampling limitations and thus researchers have been seeking alternative tools including OCT to achieve a more accurate diagnosis. A series of OCT studies conducted by Masci et al.[101,102] showed that OCT can be used to effectively differentiate celiac disease based on the OCT findings of villous atrophy. Kamboj et al.[103] reported the first case of the NvisionVLE system to identify the structural features of a duodenal neuroendocrine tumor (NET), which revealed an asymmetric submucosal mass with septated regions of high and low signal intensity corresponding to a well-circumscribed mass with multiple lobules separated by fibrous septa from the matching histology. Figure 10 shows another example of OCT applications at the other end of the small intestine, the terminal ileum (TI).[90] Recently, Lee et al.[104] used an ultrahigh-speed endoscopic OCT system to study the structural difference of Crohn's disease in the TI compared with a healthy control, and showed the TI with Crohn's ileitis exhibited irregular mucosal patterns and enlarged villi internal structures, suggesting OCT could also be a promising tool for disease diagnosis in the small intestine.

4 New Technologies and Future Applications

In addition to the GI clinical activities with the use of state-of-the-art endoscopic OCT, there are several technologies that have been developed and could be easily integrated with OCT to

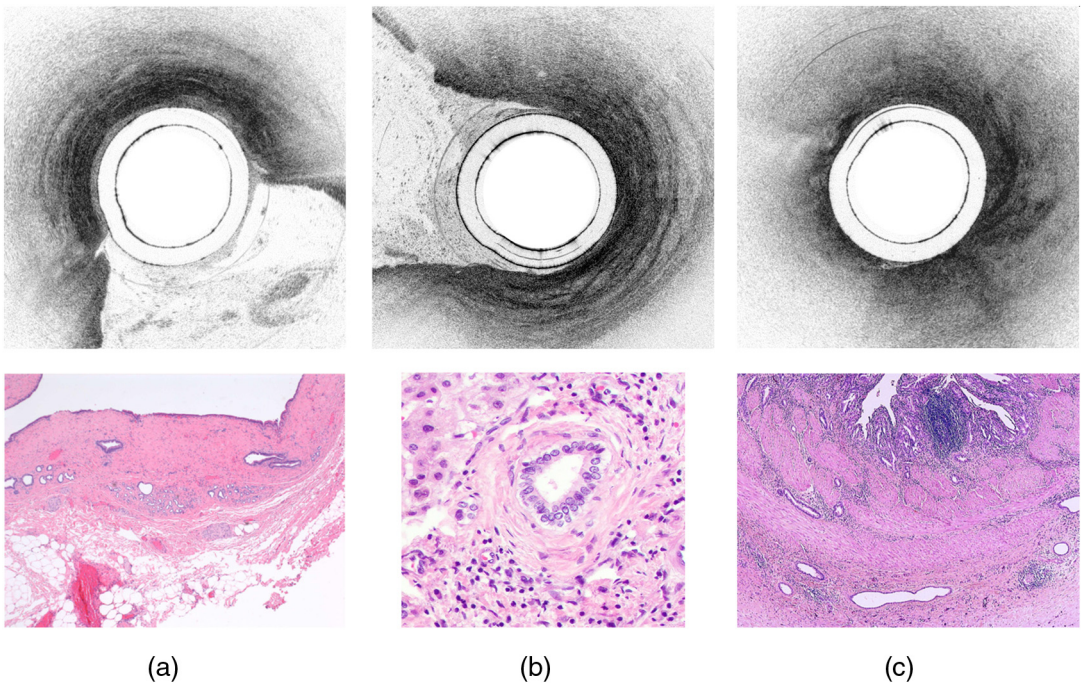

Fig. 8 Representative VLE (top) and histological (bottom) images in the biliary duct: (a) normal bile duct; (b) PSC shows in-tact wall layering, "onion-skin" structure, and subsurface hyperreflective regions; (c) cholangiocarcinoma shows hyperreflective surface, loss of ductal wall layering and image penetration, and thickened luminal debris and/or epithelial projections. Courtesy of Dr. Virendra Joshi at Ochsner Clinic Foundation, Dr. Douglas Pleskow at Beth Israel Deaconess Medical Center, and Dr. Isaac Raijman at Baylor College of Medicine.

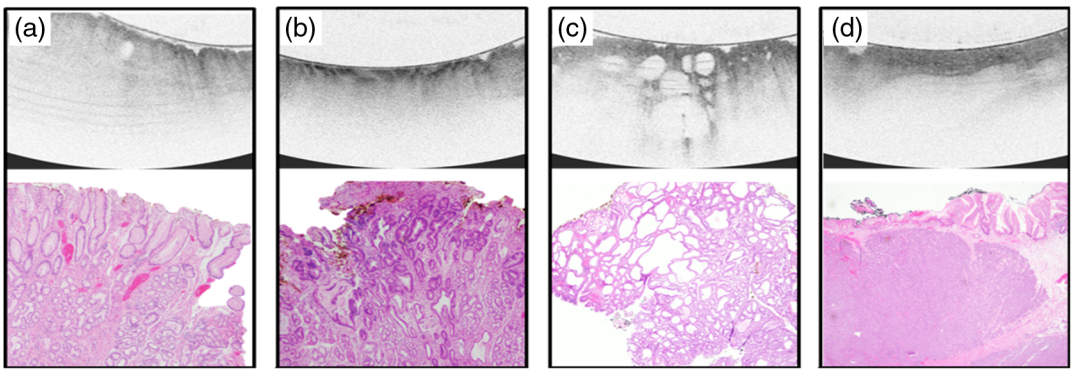

Fig. 9 OCT findings in normal and diseased gastric tissue: (a) normal gastric tissue has a regular foveolar appearance with characteristic "pits" and "crypts" presenting as superficial striations in the image; (b) in focal intestinal metaplasia shows a disruption to the normal pits and crypts structure along with increased surface reflectivity; (c) gastric adenoma presents as a loss of pit and crypt structure with a proliferation of clustered, dilated atypical glands; (d) NET of the stomach presents as a loss of pit and crypt structure with a distinct, low scattering submucosal structure, clearly delineated from surrounding tissue. Original published in Ref. 98.

achieve better performance or provide additional functionality. This section will discuss a few examples and the new opportunities for GI applications with the use of these integrated/advanced OCT technologies.

4.1 *Endoscopic Optical Coherence Tomography Angiography for Microvasculature Visualization*

Vascular patterns on the surface of a lesion are another important indicator in detecting dysplasia in the GI tract. Imaging technologies that can enhance the surface vascular contrast, such as chromoendoscopy or NBI combined with magnification endoscopy, have been demonstrated to provide high sensitivity for detection of HGD.[34,105] Phase or intensity variation-based OCT techniques have been developed to image microvasculature networks without the need for exogenous contrast agents,[106–112] but these techniques were challenging to implement in a probe-based OCT setting because dense sampling and high frame-to-frame scanning stability is critical to resolve the microvasculature with high sensitivity. The ultrahigh-speed endoscopic OCT system with a distal scanning probe was able to

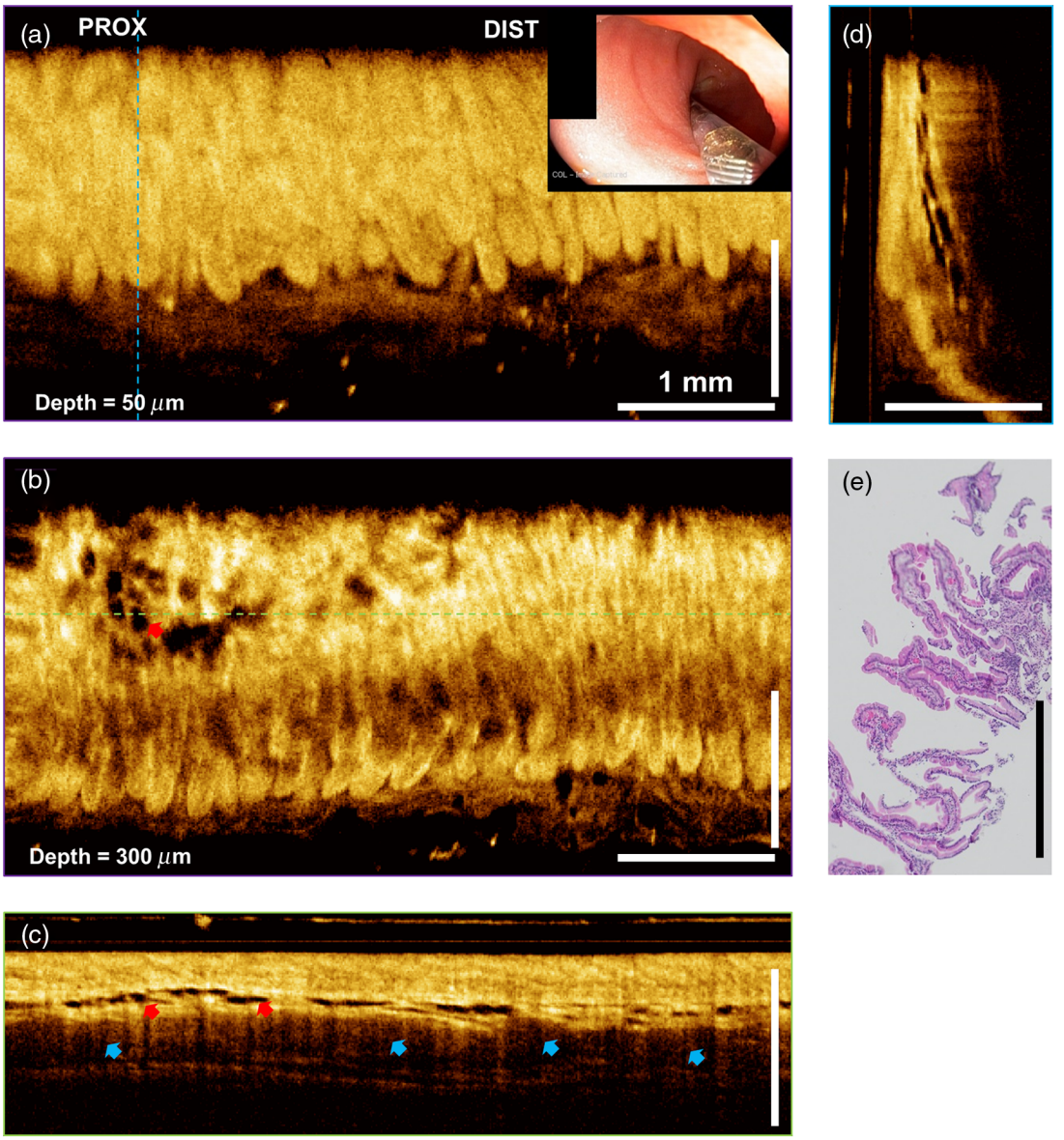

Fig. 10 Volumetric OCT of the terminal ileum: (a) *en face* OCT image at 50-μm depth shows typical villi structure. The inset shows the endoscopic view of the terminal ileum with the OCT imaging catheter in contact with the ileum wall; (b) *en face* OCT image at 300-μm depth shows numerous glandular structures under the tissue surface; (c) cross-sectional image along the pullback direction; (d) cross-sectional image along the rotary direction; (e) corresponding biopsy histology of the terminal ileum. Red arrow: ileum glands. Blue arrows: Peyer's patches. Originally published in Ref. 99.

overcome these challenges and Tsai et al.[113] reported the first human OCT angiography (OCTA) of the GI tract that revealed clear differentiation of microvasculature between normal tissue and BE (Fig. 11). The system was later used to conduct a series of clinical studies, including a 52-patient study to investigate the microvasculature features associated with dysplastic BE,[114] opening up a new regime for endoscopic OCT-based research.

4.2 *Optical Coherence Elastography for Quantifying Tissue Mechanical Properties*

High speed and high resolution allows OCT to visualize small displacements of tissue due to external forces, and can be used to quantify mechanical properties, such as strain and elasticity.[115,116] With disease progression, mechanical properties of tissue can change due to different cell type composition. Researchers have developed OCT-based methods to quantify these changes, namely optical coherence elastography (OCE).[117] Most of the development efforts focused on the methods to induce tissue displacement effectively, and to develop signal processing algorithms to optimize sensitivity,[118–120] OCE was used to study human breast tumor,[121] and assess breast cancer margins[122] with promising early results. Probe-based OCE has been demonstrated in a forward-viewing configuration mainly due to the need to introduce tissue displacement with the probe contact.[123,124] This requirement may limit the endoscopic OCE applications to be point-based examination, but further research and innovation are needed.

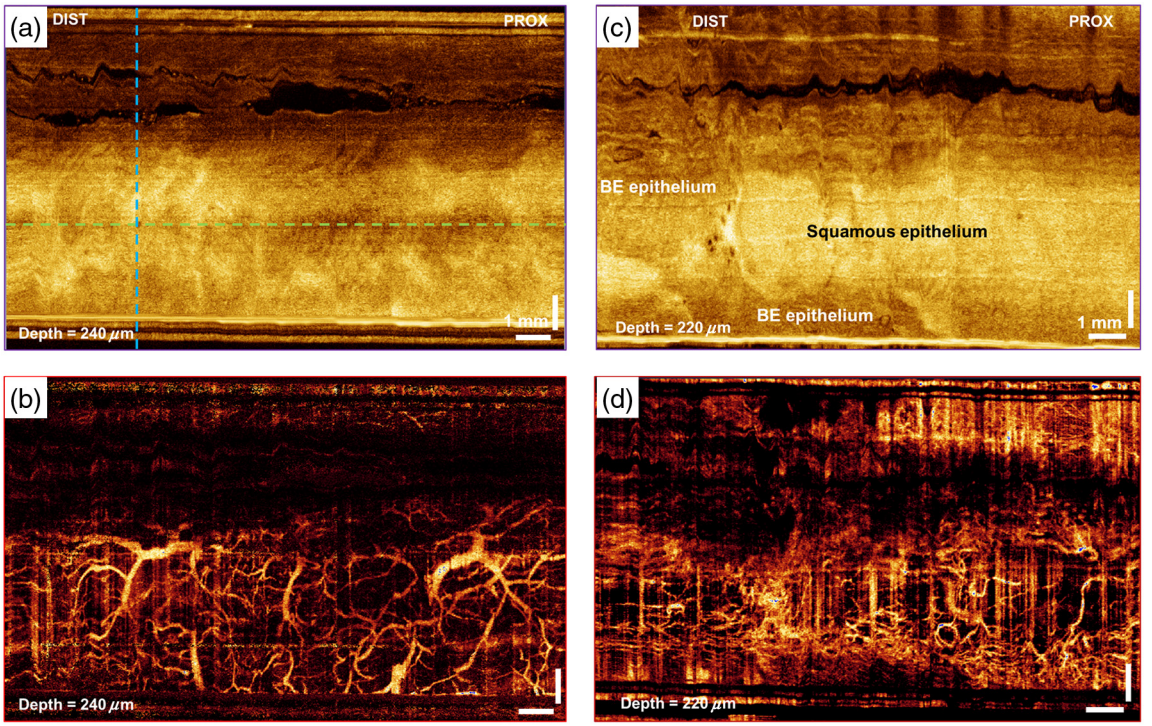

Fig. 11 OCT angiography reveals microvasculature in normal and BE: (a) *en face* intensity image at the imaging depth of 240 μm of the normal esophagus, corresponding to the lamina propria layer; (b) OCT angiogram in the same layer significantly enhances the contrast of the microvasculature in lamina propria; (c) *en face* intensity image at the imaging depth of 220 μm of a nondysplastic BE, corresponding to the lamina propria layer; (d) OCT angiogram in the same layers shows dense vascular structure along the squamous–columnar junction, which may be an indication of BE progression. Originally published in Ref. 113.

4.3 *Polarization-Sensitive Optical Coherence Tomography Provides Additional Tissue Contrast*

Polarization-sensitive OCT (PS-OCT) can measure the change in polarization as light penetrates tissue with birefringence[125,126] and has been broadly used in free-space bench-top applications such as ophthalmology to study the birefringence properties of biological tissues.[127–130] To be used in fiber optics probe-based OCT applications, researchers have developed several solutions to correct the change of polarization state within the probes by modulating the polarization modulation in the OCT interferometer.[131–133] Probe-based PS-OCT has been utilized clinically in cardiology[134] and pulmonology,[135] and shown to clearly reveal additional tissue contrast such as collagen fibers and smooth muscle on top of the OCT structural images. Although there currently are no publications demonstrating *in vivo* PS-OCT data from the GI tract, the capability to highlight muscular structures is a relevant addition to intensity-based OCT images, as the distribution of muscularis mucosa is another indicator to differentiate disease in the GI tract. Although muscularis mucosa is typically a thin layer between the lamina propria and submucosa, it is sometimes challenging to delineate the muscularis mucosa layer simply based on the intensity images, so PS-OCT may provide more comprehensive information for disease diagnosis.

Figure 12 shows *in vivo* endoscopic PS-OCT images from a recent unpublished study in swine, using a modified NvisionVLE imaging system. By modulating the polarization states of consecutive sweeps from the SS and calculating the Stokes vectors rotation adopted from the methods described in Ref. 132, local retardation (LR, represents birefringence of the tissue) and degree of polarization uniformity (DOPU, represents scattering from tissue structure) were measured in a live swine esophagus. From the LR image, the layers consist of muscle fiber, including muscularis mucosa and muscularis propria, showing higher local retardation values corresponding to higher birefringence. Connective tissue layers including lamina propria and submucosa show relatively low LR values, and the epithelium layer basically presents no LR. From the DOPU image, epithelium, lamina propria, and submucosa layers show high uniformity, whereas the muscle layers show more depolarization nature. This result demonstrates that PS-OCT offers birefringence contrast of the GI tract in an *in vivo* endoscopic setting and may become important for tissue differentiation.

4.4 *Multimodality Systems for Functional Imaging*

In addition to OCT-derivative technologies, the compact form factor of fiber-optics based probe allows easy integration of endoscopic OCT with other modalities and tools. Ultrasound has the advantage of deeper imaging penetration in tissue and is suitable for applications that require morphological information on a larger scale, such as cancer staging.[136] The integration of OCT and ultrasound can provide a full portfolio of tissue structural information and has been demonstrated in cardiovascular applications in miniaturized probe-based settings,[137,138] so it would be feasible to apply the technology for GI imaging.

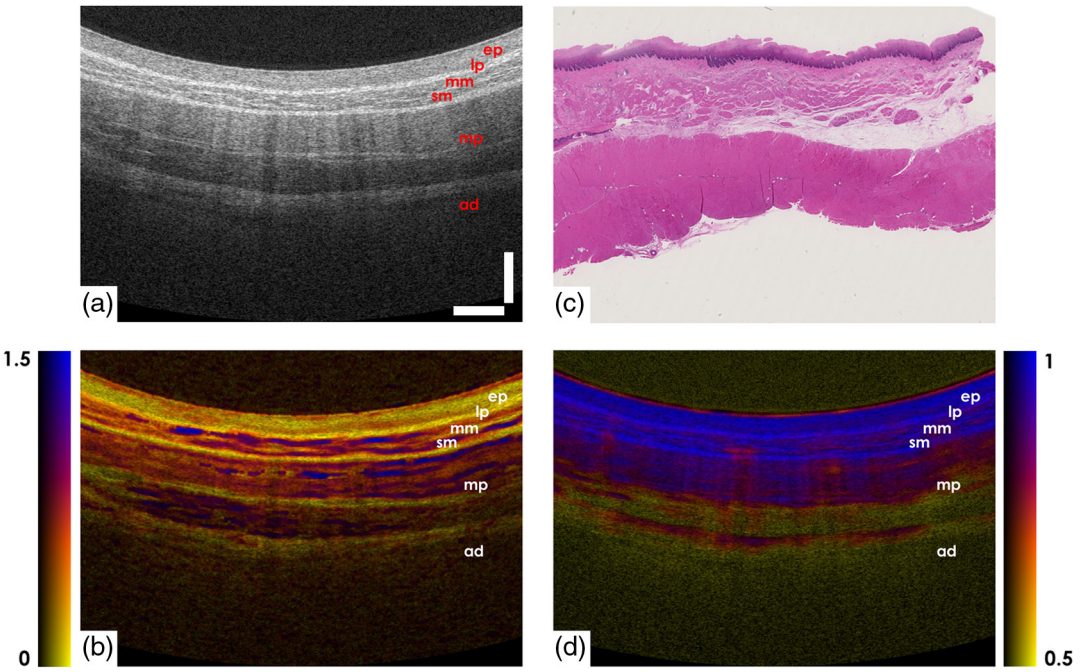

Fig. 12 *In vivo* swine esophagus images using probe-based polarization sensitive OCT: (a) intensity image shows well-defined layered structure in the normal swine esophagus; (b) corresponding histology from the imaged location; (c) intensity mapped local retardation image highlights the layers containing muscle fibers; (d) intensity mapped degree of polarization uniformity shows lower polarization uniformity in muscle layers. The color scales from 0 to 1.5 deg/μm for local retardation image and 0.5 to 1 for degree of polarization uniformity, respectively. ep, epithelium; lp, lamina propria; mm, muscularis mucosa; sm, submucosa; mp, muscularis propria. Scale bar: 1 mm. Images provided by NinePoint Medical.

Due to generally larger lumen size in the GI tract, the OCT/ultrasound probe will either operate directly in contact with the tissue or in an index-matching condition to minimize the ultrasonic signal saturation from the tissue/air interface. Similar to ultrasound, photoacoustic tomography (PAT) detects laser-induced ultrasound waves from the tissue and is extremely sensitive to optical absorbers such as hemoglobin and melanin, so it is an ideal tool to see the blood vessels. Combined PAT and OCT systems have been demonstrated in dermatological applications[139,140] and realized in probe format for endoscopic applications.[141,142] PAT can also be used to quantify hemodynamic functions such as oxygen saturation and hemoglobin concentration, which can serve as a potential biomarker for disease differentiation.[143,144]

The use of fiber optics allows transmitting light with different wavelengths simultaneously and thus fluorescence imaging is another modality that can operate alongside OCT. Fluorescent contrasts offer molecular information from the tissue complementary to OCT's structural information and thus could improve the specificity. Various research groups have demonstrated the feasibility of combined fluorescence and OCT imaging in probe-based settings in pulmonary nodule detection,[145,146] coronary artery disease assessment,[147–149] vasculature detection in the esophagus,[150] and fundamental biology research.[151]

As endoscopic OCT is able to guide tissue sampling and therapy, it makes sense to integrate with other endoscopic tools such as tissue retrieval and ablation devices. Feasibility demonstrations of probe-based OCT with aspiration needles for pulmonary application have been shown,[152–154] as well as laser coagulation[155] and RFA[69] devices. Although there is more work to be done for the GI application space, the integration of OCT and endoscopic tools is envisioned to help simplify the clinical workflow and greatly improve the diagnostic and treatment efficacy.

5 Outlook of Endoscopic Optical Coherence Tomography

Endoscopic OCT has grown significantly over the past decade and there are many opportunities not yet fully explored in the GI space. With its high resolution, wide-area, subsurface imaging capabilities, endoscopic OCT has the potential to provide solutions to significant unmet needs in the gastroenterology practice including targeted tissue sampling as well as integration with therapy to increase diagnostic yield, guiding more effective treatment and monitoring progression of disease post treatment.

As with all new technologies, a period of investigation to evaluate the utility is followed by a period of consolidation to implement standardized techniques and workflow within a routine clinical setting. For endoscopic applications of OCT, image interpretation poses the greatest level of effort in this standardization process. As the technology is more widely accessible, such as the case with esophageal OCT imaging, studies investigating the relationship between image features and the underlying pathology, development of clinically relevant algorithms for diagnosis of specific conditions, and finally standardized methods for training and dissemination are ongoing.[53,57,114,156,157]

With the advancement of image processing and machine learning techniques, the ability to perform real-time automated

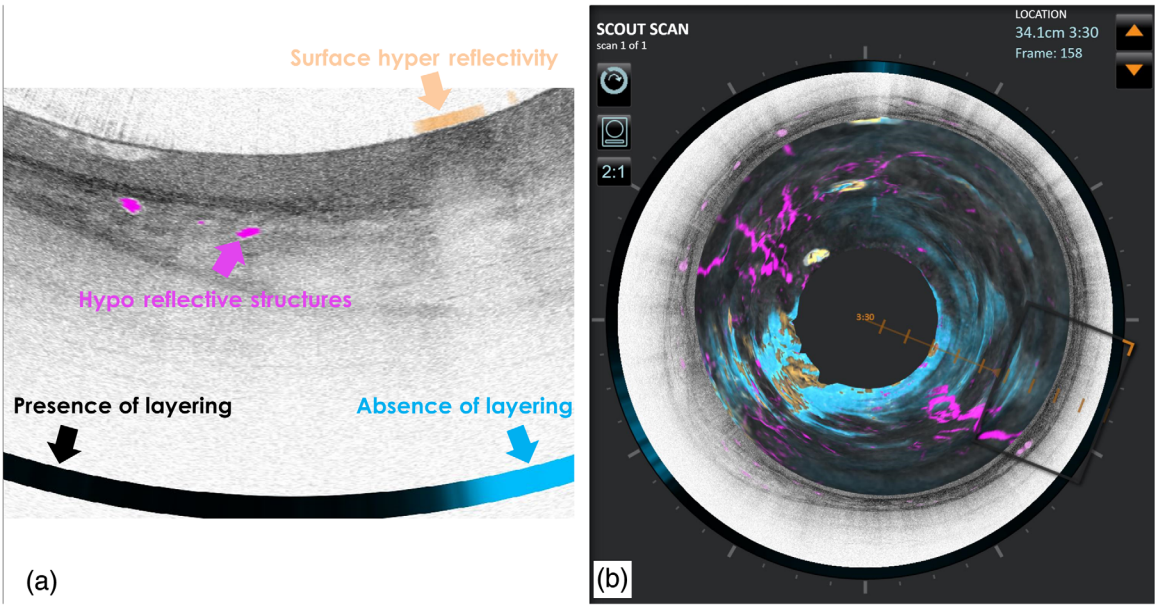

Fig. 13 An example machine learning algorithm identifying specific OCT image features within the esophagus, including tissue surface hyperreflectivity, layering, and hyporeflective structures. (a) Cross-sectional view shows all three features highlighted. (b) Luminal view shows the features overlaid on the volumetric dataset. Images provided by NinePoint Medical.

detection and diagnosis of suspicious regions within these large volumetric OCT datasets is now within reach. Recently, multiple groups have published such computer-aided algorithms for detection of esophageal diseases using OCT[158–162] and demonstrated high diagnostic accuracy. Figure 13 shows an example machine learning algorithm that can identify specific OCT image features within the esophagus, including tissue surface hyperreflectivity, layering, and hyporeflective structures. We believe that further research and development in this field will transform OCT into a routine clinical tool for real-time disease guidance and management.

In conclusion, endoscopic OCT is a unique technology that provides high resolution, minimally invasive optical sectioning in 3-D while being able to support broad imaging coverage. Collaboration and innovation from both academia and industry have contributed to the commercialization of this technology, with continued effort we believe endoscopic OCT will further advance the gastroenterology practice and improve patient quality of life.

Disclosures

T.-H. Tsai and E. Namati are under direct employment of NinePoint Medical, Inc. All other authors disclosed no financial relationships relevant to this publication.

Acknowledgments

The authors would like to thank the clinical, marketing, and R&D team members of NinePoint Medical for preparing some of the publication figures.

References

1. E. Seward and S. Lumley, "Endoscopy provision: meeting the challenges," *Frontline Gastroenterol.* **8**(2), 90–93 (2017).
2. N. Kurniawan and M. Keuchel, "Flexible gastro-intestinal endoscopy—clinical challenges and technical achievements," *Comput. Struct. Biotechnol. J.* **15**, 168–179 (2017).
3. D. Huang et al., "Optical coherence tomography," *Science* **254**(5035), 1178–1181 (1991).
4. G. J. Tearney et al., "*In vivo* endoscopic optical biopsy with optical coherence tomography," *Science* **276**(5321), 2037–2039 (1997).
5. E. A. Swanson et al., "*In vivo* retinal imaging by optical coherence tomography," *Opt. Lett.* **18**(21), 1864–1866 (1993).
6. A. F. Fercher et al., "Measurement of intraocular distances by backscattering spectral interferometry," *Opt. Commun.* **117**(1–2), 43–48 (1995).
7. B. Cense et al., "Ultrahigh-resolution high-speed retinal imaging using spectral-domain optical coherence tomography," *Opt. Express* **12**(11), 2435–2447 (2004).
8. M. Wojtkowski et al., "Ophthalmic imaging by spectral optical coherence tomography," *Am. J. Ophthalmol.* **138**(3), 412–419 (2004).
9. K. Takada et al., "New measurement system for fault location in optical waveguide devices based on an interferometric technique," *Appl. Opt.* **26**(9), 1603–1608 (1987).
10. H. H. Gilgen et al., "Submillimeter optical reflectometry," *IEEE J. Lightwave Technol.* **7**(8), 1225–1233 (1989).
11. E. A. Swanson et al., "High-speed optical coherence domain reflectometry," *Opt. Lett.* **17**(2), 151–153 (1992).
12. M. A. Choma et al., "Sensitivity advantage of swept source and Fourier domain optical coherence tomography," *Opt. Express* **11**(18), 2183–2189 (2003).
13. J. F. de Boer et al., "Improved signal-to-noise ratio in spectral-domain compared with time-domain optical coherence tomography," *Opt. Lett.* **28**(21), 2067–2069 (2003).
14. R. Leitgeb, C. K. Hitzenberger, and A. F. Fercher, "Performance of Fourier domain vs. time domain optical coherence tomography," *Opt. Express* **11**(8), 889–894 (2003).
15. N. Nassif et al., "In vivo human retinal imaging by ultrahigh-speed spectral domain optical coherence tomography," *Opt. Lett.* **29**(5), 480–482 (2004).
16. S. R. Chinn, E. A. Swanson, and J. G. Fujimoto, "Optical coherence tomography using a frequency-tunable optical source," *Opt. Lett.* **22**(5), 340–342 (1997).
17. S. H. Yun et al., "High-speed wavelength-swept semiconductor laser with a polygon-scanner-based wavelength filter," *Opt. Lett.* **28**(20), 1981–1983 (2003).

18. T. H. Ko et al., "Ultrahigh resolution optical coherence tomography imaging with a broadband superluminescent diode light source," *Opt. Express* **12**(10), 2112–2119 (2004).
19. F. E. Robles, S. Chowdhury, and A. Wax, "Assessing hemoglobin concentration using spectroscopic optical coherence tomography for feasibility of tissue diagnostics," *Biomed. Opt. Express* **1**(1), 310–317 (2010).
20. B. J. Vakoc et al., "Comprehensive esophageal microscopy by using optical frequency-domain imaging (with video)," *Gastrointest. Endoscopy* **65**(6), 898–905 (2007).
21. D. C. Adler et al., "Three-dimensional endomicroscopy using optical coherence tomography," *Nat. Photonics* **1**(12), 709–716 (2007).
22. T.-H. Tsai et al., "Piezoelectric-transducer-based miniature catheter for ultrahigh-speed endoscopic optical coherence tomography," *Biomed. Opt. Express* **2**(8), 2438–2448 (2011).
23. W. Wieser et al., "Multi-megahertz OCT: high quality 3D imaging at 20 million A-scans and 4.5 GVoxels per second," *Opt. Express* **18**(14), 14685–14704 (2011).
24. T. Wang et al., "Heartbeat OCT and motion-free 3D *in vivo* coronary artery microscopy," *JACC: Cardiovasc. Imaging* **9**(5), 622 (2016).
25. T.-H. Tsai, J. Fujimoto, and H. Mashimo, "Endoscopic optical coherence tomography for clinical gastroenterology," *Diagnostics* **4**(2), 57–93 (2014).
26. M. J. Gora et al., "Endoscopic optical coherence tomography: technologies and clinical applications [Invited]," *Biomed. Opt. Express* **8**(5), 2405–2444 (2017).
27. M. J. Suter et al., "Comprehensive microscopy of the esophagus in human patients with optical frequency domain imaging," *Gastrointest. Endoscopy* **68**(4), 745–753 (2008).
28. M. J. Gora et al., "Tethered capsule endomicroscopy enables less invasive imaging of gastrointestinal tract microstructure," *Nat. Med.* **19**(2), 238–240 (2013).
29. Y. T. Pan, H. K. Xie, and G. K. Fedder, "Endoscopic optical coherence tomography based on a microelectromechanical mirror," *Opt. Lett.* **26**(24), 1966–1968 (2001).
30. E. J. Seibel and Q. Y. J. Smithwick, "Unique features of optical scanning, single fiber endoscopy," *Lasers Surg. Med.* **30**(3), 177–183 (2002).
31. S. Moon et al., "Semi-resonant operation of a fiber-cantilever piezotube scanner for stable optical coherence tomography endoscope imaging," *Opt. Express* **18**(20), 21183–21197 (2010).
32. American Cancer Society, "Cancer facts and figures—2017," American Cancer Society, Atlanta (2017).
33. S. E. Kudo et al., "Diagnosis of colorectal tumorous lesions by magnifying endoscopy," *Gastrointest. Endoscopy* **44**(1), 8–14 (1996).
34. P. Sharma et al., "The utility of a novel narrow band imaging endoscopy system in patients with Barrett's esophagus," *Gastrointest. Endoscopy* **64**(2), 167–175 (2006).
35. R. F. Souza, C. P. Morales, and S. J. Spechler, "Review article: a conceptual approach to understanding the molecular mechanisms of cancer development in Barrett's oesophagus," *Aliment. Pharmacol. Ther.* **15**(8), 1087–1100 (2001).
36. A. P. Weston et al., "p53 protein overexpression in low grade dysplasia (LGD) in Barrett's esophagus: immunohistochemical marker predictive of progression," *Am. J. Gastroenterol.* **96**(5), 1355–1362 (2001).
37. N. J. Shaheen et al., "ACG clinical guideline: diagnosis and management of Barrett's esophagus," *Am. J. Gastroenterol.* **111**(1), 30–50 (2016).
38. P. T. Chandrasoma and T. R. DeMeester, *GERD: Reflux to Esophageal Adenocarcinoma*, Elsevier Science (2010).
39. H. Mashimo, M. S. Wagh, and R. K. Goyal, "Surveillance and screening for Barrett esophagus and adenocarcinoma," *J. Clin. Gastroenterol.* **39**(4), S33–S41 (2005).
40. M. A. Anderson et al., "Complications of ERCP," *Gastrointest. Endoscopy* **75**(3), 467–473 (2012).
41. H. Inoue and M. Endo, "Endoscopic esophageal mucosal resection using a transparent tube," *Surg. Endoscopy* **4**(4), 198–201 (1990).
42. T. Oyama et al., "Endoscopic submucosal dissection of early esophageal cancer," *Clin. Gastroenterol. Hepatol.* **3**(7, Suppl. 1), S67–S70 (2005).
43. M. Hirao et al., "Endoscopic resection of early gastric cancer and other tumors with local injection of hypertonic saline-epinephrine," *Gastrointest. Endoscopy* **34**(3), 264–269 (1988).
44. K. E. Grund, D. Storek, and G. Farin, "Endoscopic argon plasma coagulation (APC) first clinical experiences in flexible endoscopy," *Endoscopic Surg. Allied Technol.* **2**(1), 42–46 (1994).
45. N. J. Shaheen et al., "Radiofrequency ablation in Barrett's esophagus with dysplasia," *New Engl. J. Med.* **360**(22), 2277–2288 (2009).
46. M. H. Johnston et al., "Cryoablation of Barrett's esophagus: a pilot study," *Gastrointest. Endoscopy* **62**(6), 842–848 (2005).
47. S. Friedland and G. Triadafilopoulos, "A novel device for ablation of abnormal esophageal mucosa (with video)," *Gastrointest. Endoscopy* **74**(1), 182–188 (2011).
48. K. K. Wang and R. E. Sampliner, "Updated guidelines 2008 for the diagnosis, surveillance and therapy of Barrett's esophagus," *Am. J. Gastroenterol.* **103**(3), 788–797 (2008).
49. T.-H. Tsai et al., "Length of proximal extent of subsquamous intestinal metaplasia correlates with difficult eradication of Barrett esophagus by radiofrequency ablation," *Gastroenterology* **144**(5), S-174 (2013).
50. A. F. Swager et al., "Detection of buried Barrett's glands after radiofrequency ablation with volumetric laser endomicroscopy," *Gastrointest. Endoscopy* **83**(1), 80–88 (2016).
51. C. L. Leggett et al., "Volumetric laser endomicroscopy detects subsquamous Barrett's adenocarcinoma," *Am. J. Gastroenterol.* **109**(2), 298–299 (2014).
52. J. M. Poneros et al., "Diagnosis of specialized intestinal metaplasia by optical coherence tomography," *Gastroenterology* **120**(1), 7–12 (2001).
53. J. A. Evans et al., "Identifying intestinal metaplasia at the squamocolumnar junction by using optical coherence tomography," *Gastrointest. Endoscopy* **65**(1), 50–56 (2007).
54. J. A. Evans et al., "Optical coherence tomography to identify intramucosal carcinoma and high-grade dysplasia in Barrett's esophagus," *Clin. Gastroenterol. Hepatol.* **4**(1), 38–43 (2006).
55. A. J. Trindade, A. S. Vamadevan, and D. V. Sejpal, "Finding a needle in a haystack: use of volumetric laser endomicroscopy in targeting focal dysplasia in long-segment Barrett's esophagus," *Gastrointest. Endoscopy* **82**(4), 756–757 (2015).
56. M. S. Smith et al., "Volumetric laser endomicroscopy improves patient management by enhancing detection and sampling of esophageal histopathology: results from the interim analysis of a multi-center registry," *Gastroenterology* **150**(4), S55–S56 (2016).
57. C. L. Leggett et al., "Comparative diagnostic performance of volumetric laser endomicroscopy and confocal laser endomicroscopy in the detection of dysplasia associated with Barrett's esophagus," *Gastrointest. Endoscopy* **83**(5), 880–888 (2016).
58. A.-F. Swager et al., "Identification of volumetric laser endomicroscopy features predictive for early neoplasia in Barrett's esophagus using high-quality histological correlation," *Gastrointest. Endoscopy* **85**(5), 918–926 (2017).
59. P. Sharma et al., "The American society for gastrointestinal endoscopy PIVI (Preservation and Incorporation of Valuable Endoscopic Innovations) on imaging in Barrett's esophagus," *Gastrointest. Endoscopy* **76**(2), 252–254 (2012).
60. M. J. Bartel et al., "Subsquamous intestinal metaplasia is common in treatment-naïve Barrett's esophagus," *Gastrointest. Endoscopy* (2017).
61. M. J. Suter et al., "Image-guided biopsy in the esophagus through comprehensive optical frequency domain imaging and laser marking: a study in living swine," *Gastrointest. Endoscopy* **71**(2), 346–353 (2010).
62. A. F. Swager et al., "Feasibility of laser marking in Barrett's esophagus with volumetric laser endomicroscopy: first-in-man pilot study," *Gastrointest. Endoscopy* **86**(3), 464–472 (2017).
63. L. A. Torre et al., "Global cancer statistics, 2012," *CA: Cancer J. Clin.* **65**(2), 87–108 (2015).
64. W. Hatta et al., "Optical coherence tomography for the staging of tumor infiltration in superficial esophageal squamous cell carcinoma," *Gastrointest. Endoscopy* **71**(6), 899–906 (2010).
65. W. Hatta et al., "A prospective comparative study of optical coherence tomography and EUS for tumor staging of superficial esophageal squamous cell carcinoma," *Gastrointest. Endoscopy* **76**(3), 548–555 (2012).
66. A. J. Trindade et al., "Use of volumetric laser endomicroscopy in staging multifocal superficial squamous carcinoma of the esophagus," *Gastrointest. Endoscopy* **84**(2), 369 (2016).

67. T.-H. Tsai et al., "Structural markers observed with endoscopic 3-dimensional optical coherence tomography correlating with Barrett's esophagus radiofrequency ablation treatment response," *Gastrointest. Endoscopy* **76**(6), 1104–1112 (2012).
68. T.-H. Tsai et al., "Comparison of tissue architectural changes between radiofrequency ablation and cryospray ablation in Barrett's esophagus using endoscopic three-dimensional optical coherence tomography," *Gastroenterol. Res. Pract.* **2012**, 1–8 (2012).
69. H. C. Lee et al., "Assessment of the radiofrequency ablation dynamics of esophageal tissue with optical coherence tomography," *J. Biomed. Opt.* **22**(7), 076001 (2017).
70. C. Zhou et al., "Characterization of buried glands before and after radiofrequency ablation by using 3-dimensional optical coherence tomography (with videos)," *Gastrointest. Endoscopy* **76**(1), 32–40 (2012).
71. D. E. Fleischer et al., "Endoscopic radiofrequency ablation for Barrett's esophagus: 5-year outcomes from a prospective multicenter trial," *Endoscopy* **42**, 781–789 (2010).
72. N. J. Shaheen et al., "Durability of radiofrequency ablation in Barrett's esophagus with dysplasia," *Gastroenterology* **141**(2), 460–468 (2011).
73. M. Gupta et al., "Recurrence of esophageal intestinal metaplasia after endoscopic mucosal resection and radiofrequency ablation of Barrett's esophagus: results from a US Multicenter Consortium," *Gastroenterology* **145**(1), 79-86.e71 (2013).
74. T. J. Hayeck et al., "The prevalence of Barrett's esophagus in the US: estimates from a simulation model confirmed by SEER data," *Dis. Esophagus* **23**(6), 451–457 (2010).
75. F. Hvid-Jensen et al., "Incidence of adenocarcinoma among patients with Barrett's esophagus," *New England J. Med.* **365**(15), 1375–1383 (2011).
76. S. Bhat et al., "Risk of malignant progression in Barrett's esophagus patients: results from a large population-based study," *J. Natl. Cancer Institute* **103**(13), 1049–1057 (2011).
77. D. K. Rex et al., "Screening for Barrett's esophagus in colonoscopy patients with and without heartburn," *Gastroenterology* **125**(6), 1670–1677 (2003).
78. M. J. Gora et al., "Imaging the upper gastrointestinal tract in unsedated patients using tethered capsule endomicroscopy," *Gastroenterology* **145**(4), 723–725 (2013).
79. M. J. Gora et al., "Tethered capsule endomicroscopy: from bench to bedside at a primary care practice," *J. Biomed. Opt.* **21**(10), 104001 (2016).
80. K. Liang et al., "Ultrahigh speed en face OCT capsule for endoscopic imaging," *Biomed. Opt. Express* **6**(4), 1146–1163 (2015).
81. K. Liang et al., "Volumetric mapping of Barrett's esophagus and dysplasia with en face optical coherence tomography tethered capsule," *Am. J. Gastroenterol.* **111**(11), 1664–1666 (2016).
82. P. R. Pfau et al., "Criteria for the diagnosis of dysplasia by endoscopic optical coherence tomography," *Gastrointest. Endoscopy* **58**(2), 196–202 (2003).
83. E. Zagaynova et al., "Endoscopic OCT with forward-looking probe: clinical studies in urology and gastroenterology," *J. Biophotonics* **1**(2), 114–128 (2008).
84. B. Shen et al., "*In vivo* colonoscopic optical coherence tomography for transmural inflammation in inflammatory bowel disease," *Clin. Gastroenterol. Hepatol.* **2**(12), 1080–1087 (2004).
85. P. Consolo et al., "Optical coherence tomography in inflammatory bowel disease: Prospective evaluation of 35 patients," *Dis. Colon Rectum* **51**(9), 1374–1380 (2008).
86. A. J. Trindade et al., "Successful use of volumetric laser endomicroscopy in imaging a rectal polyp," *Ther. Adv. Gastroenterol.* **9**(1), 128–131 (2016).
87. D. C. Adler et al., "Three-dimensional endomicroscopy of the human colon using optical coherence tomography," *Opt. Express* **17**(2), 784–796 (2009).
88. K. Liang et al., "Endoscopic forward-viewing optical coherence tomography and angiography with MHz swept source," *Opt. Lett.* **42**(16), 3193–3196 (2017).
89. V. Pugliese et al., "Pancreatic intraductal sampling during ERCP in patients with chronic pancreatitis and pancreatic cancer: cytologic studies and K-RAS-2 codon 12 molecular analysis in 47 cases," *Gastrointest. Endoscopy* **54**(5), 595–599 (2001).
90. T. Rosch et al., "ERCP or EUS for tissue diagnosis of biliary strictures? A prospective comparative study," *Gastrointest. Endoscopy* **60**(3), 390–396 (2004).
91. S. M. Selvaggi, "Biliary brushing cytology," *Cytopathology* **15**(2), 74–79 (2004).
92. M. de Bellis et al., "Tissue sampling at ERCP in suspected malignant biliary strictures (Part 2)," *Gastrointest. Endoscopy* **56**(5), 720–730 (2002).
93. U. Seitz et al., "First *in vivo* optical coherence tomography in the human bile duct," *Endoscopy* **33**(12), 1018–1021 (2001).
94. J. M. Poneros et al., "Optical coherence tomography of the biliary tree during ERCP," *Gastrointest. Endoscopy* **55**(1), 84–88 (2002).
95. P. A. Testoni et al., "Intraductal optical coherence tomography for investigating main pancreatic duct strictures," *Am. J. Gastroenterol.* **102**(2), 269–274 (2007).
96. A. Tyberg et al., "Second generation optical coherence tomography: preliminary experience in pancreatic and biliary strictures," *Gastroenterology* **152**(5), S1032–S1033 (2017).
97. V. Joshi et al., "A pilot study of safety and efficacy of directed cannulation with a low profile catheter (LP) and imaging characteristics of bile duct wall using optical coherance tomography (OCT) for Indeterminate biliary strictures initial report on in-vivo evaluation during ERCP," *Gastrointest. Endoscopy* **85**(5), AB496–AB497 (2017).
98. M.-M. Xu, S. M. Lagana, and A. Sethi, "Use of optical coherence tomography (OCT) in the evaluation of gastric lesions," *Gastrointest. Endoscopy* **81**(5), AB462–AB463 (2015).
99. T.-H. Tsai et al., "Ultrahigh speed endoscopic optical coherence tomography for gastroenterology," *Biomed. Opt. Express* **5**(12), 4387–4404 (2014).
100. H.-C. Lee et al., "Novel ultrahigh speed endoscopic OCT angiography identifies both architectural and microvascular changes in patients with Gastric Antral Vascular Ectasia (GAVE) undergoing Radiofrequency Ablation (RFA) treatment," *Gastroenterology* **150**(4), S435–S436 (2016).
101. E. Masci et al., "Pilot study on the correlation of optical coherence tomography with histology in celiac disease and normal subjects," *J. Gastroenterol. Hepatol.* **22**(12), 2256–2260 (2007).
102. E. Masci et al., "Optical coherence tomography in pediatric patients: a feasible technique for diagnosing celiac disease in children with villous atrophy," *Digest. Liver Dis.* **41**(9), 639–643 (2009).
103. A. K. Kamboj et al., "Use of volumetric laser endomicroscopy to characterize a duodenal neuroendocrine tumor," *Gastrointest. Endoscopy* (In Press).
104. H.-C. Lee et al., "Endoscopic optical coherence tomography microangiography identifies the altered microvasculature of the terminal ileum in Crohn's disease," *Gastrointest. Endoscopy* **85**(5), AB511–AB512 (2017).
105. R. Singh et al., "Narrow-band imaging with magnification in Barrett's esophagus: validation of a simplified grading system of mucosal morphology patterns against histology," *Endoscopy* **40**(6), 457–463 (2008).
106. J. A. Izatt et al., "*In vivo* bidirectional color Doppler flow imaging of picoliter blood volumes using optical coherence tomography," *Opt. Lett.* **22**(18), 1439–1441 (1997).
107. V. X. Yang et al., "Endoscopic Doppler optical coherence tomography in the human GI tract: initial experience," *Gastrointest. Endoscopy* **61**(7), 879–890 (2005).
108. S. Makita et al., "Optical coherence angiography," *Opt. Express* **14**(17), 7821–7840 (2006).
109. R. K. Wang et al., "Three dimensional optical angiography," *Opt. Express* **15**(7), 4083–4097 (2007).
110. H. W. Ren et al., "Real-time *in vivo* dblood-flow imaging by movings-catterer-sensitive spectral-domain optical Doppler tomography," *Opt. Lett.* **31**(7), 927–929 (2006).
111. A. Mariampillai et al., "Speckle variance detection of microvasculature using swept-source optical coherence tomography," *Opt. Lett.* **33**(13), 1530–1532 (2008).

112. Y. Jia et al., "Split-spectrum amplitude-decorrelation angiography with optical coherence tomography," *Opt. Express* **20**(4), 4710–4725 (2012).
113. T.-H. Tsai et al., "Endoscopic optical coherence angiography enables three dimensional visualization of subsurface microvasculature," *Gastroenterology* **147**(6), 1219–1221 (2014).
114. H. C. Lee et al., "Endoscopic optical coherence tomography angiography microvascular features associated with dysplasia in Barrett's esophagus (with video)," *Gastrointest. Endoscopy* **86**(3), 476–484 (2017).
115. J. M. Schmitt, "OCT elastography: imaging microscopic deformation and strain of tissue," *Opt. Express* **3**(6), 199–211 (1998).
116. J. Rogowska et al., "Optical coherence tomographic elastography technique for measuring deformation and strain of atherosclerotic tissues," *Heart (British Cardiac Society)* **90**(5), 556–562 (2004).
117. B. F. Kennedy et al., "*In vivo* three-dimensional optical coherence elastography," *Opt. Express* **19**(7), 6623–6634 (2011).
118. X. Liang and S. A. Boppart, "Biomechanical properties of *in vivo* human skin from dynamic optical coherence elastography," *IEEE Trans. Bio-med. Eng.* **57**(4), 953–959 (2010).
119. D. Alonso-Caneiro et al., "Assessment of corneal dynamics with high-speed swept source optical coherence tomography combined with an air puff system," *Opt. Express* **19**(15), 14188–14199 (2011).
120. D. Chavan et al., "Collecting optical coherence elastography depth profiles with a micromachined cantilever probe," *Opt. Lett.* **38**(9), 1476–1478 (2013).
121. K. M. Kennedy et al., "Quantitative micro-elastography: imaging of tissue elasticity using compression optical coherence elastography," *Sci. Rep.* **5**, 15538 (2015).
122. W. M. Allen et al., "Wide-field optical coherence micro-elastography for intraoperative assessment of human breast cancer margins," *Biomed. Opt. Express* **7**(10), 4139–4153 (2016).
123. K. M. Kennedy et al., "Needle optical coherence elastography for tissue boundary detection," *Opt. Lett.* **37**(12), 2310–2312 (2012).
124. Y. Qiu et al., "Quantitative optical coherence elastography based on fiber-optic probe for in situ measurement of tissue mechanical properties," *Biomed. Opt. Express* **7**(2), 688–700 (2016).
125. M. R. Hee et al., "Polarization-sensitive low-coherence reflectometer for birefringence characterization and ranging," *J. Opt. Soc. Am. B* **9**(6), 903–908 (1992).
126. J. F. De Boer et al., "Two-dimensional birefringence imaging in biological tissue by polarization-sensitive optical coherence tomography," *Opt. Lett.* **22**(12), 934–936 (1997).
127. J. F. de Boer et al., "Imaging thermally damaged tissue by polarization sensitive optical coherence tomography," *Opt. Express* **3**(212), 212–218 (1998).
128. C. E. Saxer et al., "High-speed fiber-based polarization-sensitive optical coherence tomography of *in vivo* human skin," *Opt. Lett.* **25**(18), 1355–1357 (2000).
129. B. Cense et al., "*In vivo* depth-resolved birefringence measurements of the human retinal nerve fiber layer by polarization-sensitive optical coherence tomography," *Opt. Lett.* **27**(18), 1610–1612 (2002).
130. W. C. Y. Lo et al., "Longitudinal, 3D imaging of collagen remodeling in murine hypertrophic scars *in vivo* using polarization-sensitive optical frequency domain imaging," *J. Invest. Dermatol.* **136**(1), 84–92 (2016).
131. W. Y. Oh et al., "High-speed polarization sensitive optical frequency domain imaging with frequency multiplexing," *Opt. Express* **16**(2), 1096–1103 (2008).
132. M. Villiger et al., "Spectral binning for mitigation of polarization mode dispersion artifacts in catheter-based optical frequency domain imaging," *Opt. Express* **21**(14), 16353–16369 (2013).
133. Z. Wang et al., "Depth-encoded all-fiber swept source polarization sensitive OCT," *Biomed. Opt. Express* **5**(9), 2931–2949 (2014).
134. J. N. van der Sijde et al., "First-in-man assessment of plaque rupture by polarization-sensitive optical frequency domain imaging *in vivo*," *Eur. Heart J.* **37**(24), 1932–1932 (2016).
135. D. C. Adams et al., "Birefringence microscopy platform for assessing airway smooth muscle structure and function *in vivo*," *Sci. Transl. Med.* **8**(359), 359ra131 (2016).
136. S. R. Puli et al., "Staging accuracy of esophageal cancer by endoscopic ultrasound: A meta-analysis and systematic review," *World J. Gastroenterol.* **14**(10), 1479–1490 (2008).
137. J. Yin et al., "Novel combined miniature optical coherence tomography ultrasound probe for *in vivo* intravascular imaging," *J. Biomed. Opt.* **16**(6), 060505 (2011).
138. Y. Li et al., "Fully integrated optical coherence tomography, ultrasound, and indocyanine green-based fluorescence tri-modality system for intravascular imaging," *Biomed. Opt. Express* **8**(2), 1036–1044 (2017).
139. L. Li et al., "Three-dimensional combined photoacoustic and optical coherence microscopy for *in vivo* microcirculation studies," *Opt. Express* **17**(19), 16450–16455 (2009).
140. B. Zabihian et al., "*In vivo* dual-modality photoacoustic and optical coherence tomography imaging of human dermatological pathologies," *Biomed. Opt. Express* **6**(9), 3163–3178 (2015).
141. L. Xi et al., "Miniature probe combining optical-resolution photoacoustic microscopy and optical coherence tomography for *in vivo* microcirculation study," *Appl. Opt.* **52**(9), 1928–1931 (2013).
142. X. Dai et al., "Miniature endoscope for multimodal imaging," *ACS Photonics* **4**(1), 174–180 (2017).
143. H. F. Zhang et al., "Imaging of hemoglobin oxygen saturation variations in single vessels *in vivo* using photoacoustic microscopy," *Appl. Phys. Lett.* **90**(5), 053901 (2007).
144. L. V. Wang, "Prospects of photoacoustic tomography," *Med. Phys.* **35**(12), 5758–5767 (2008).
145. D. Lorenser et al., "Dual-modality needle probe for combined fluorescence imaging and three-dimensional optical coherence tomography," *Opt. Lett.* **38**(3), 266–268 (2013).
146. H. Pahlevaninezhad et al., "Endoscopic Doppler optical coherence tomography and autofluorescence imaging of peripheral pulmonary nodules and vasculature," *Biomed. Opt. Express* **6**(10), 4191–4199 (2015).
147. S. Liang et al., "Intravascular atherosclerotic imaging with combined fluorescence and optical coherence tomography probe based on a double-clad fiber combiner," *J. Biomed. Opt.* **17**(7), 070501 (2012).
148. H. Yoo et al., "Intra-arterial catheter for simultaneous microstructural and molecular imaging *in vivo*," *Nat. Med.* **17**(12), 1680–1684 (2011).
149. G. J. Ughi et al., "Dual modality intravascular optical coherence tomography (OCT) and near-infrared fluorescence (NIRF) imaging: a fully automated algorithm for the distance-calibration of NIRF signal intensity for quantitative molecular imaging," *Int. J. Cardiovasc. Imaging* **31**(2), 259–268 (2015).
150. J. Mavadia et al., "An all-fiber-optic endoscopy platform for simultaneous OCT and fluorescence imaging," *Biomed. Opt. Express* **3**(11), 2851–2859 (2012).
151. J. Xi et al., "Integrated multimodal endomicroscopy platform for simultaneous en face optical coherence and two-photon fluorescence imaging," *Opt. Lett.* **37**(3), 362–364 (2012).
152. K. M. Tan et al., "Flexible transbronchial optical frequency domain imaging smart needle for biopsy guidance," *Biomed. Opt. Express* **3**(8), 1947–1954 (2012).
153. W.-C. Kuo et al., "Real-time three-dimensional optical coherence tomography image-guided core-needle biopsy system," *Biomed. Opt. Express* **3**(6), 1149–1161 (2012).
154. R. A. McLaughlin et al., "Static and dynamic imaging of alveoli using optical coherence tomography needle probes," *J. Appl. Physiol.* **113**(6), 967–974 (2012).
155. K. Beaudette et al., "Laser tissue coagulation and concurrent optical coherence tomography through a double-clad fiber coupler," *Biomed. Opt. Express* **6**(4), 1293–1303 (2015).
156. J. Sauk et al., "Interobserver agreement for the detection of Barrett's esophagus with optical frequency domain imaging," *Dig. Dis. Sci.* **58**(8), 2261–2265 (2013).
157. A. J. Trindade et al., "Volumetric laser endomicroscopy in Barrett's esophagus: interobserver agreement for interpretation of Barrett's esophagus and associated neoplasia among high-frequency users," *Gastrointest. Endoscopy* **86**(1), 133–139 (2017).
158. G. J. Ughi et al., "Automated segmentation and characterization of esophageal wall *in vivo* by tethered capsule optical coherence

tomography endomicroscopy," *Biomed. Opt. Express* **7**(2), 409–419 (2016).
159. A. K. Kamboj et al., "Detection of Barrett's esophagus dysplasia using a novel volumetric laser endomicroscopy computer algorithm," *Gastrointest. Endoscopy* **85**(5), AB518 (2017).
160. E. Rodriguez-Diaz and S. K. Singh, "Computer-assisted analysis of hypo-scattering glandular structures in Barrett's dysplasia observed by volumetric laser endomicroscopy," *Gastroenterology* **152**(5), S840 (2017).
161. A. F. Swager et al., "Quantitative attenuation analysis for identification of early Barrett's neoplasia in volumetric laser endomicroscopy," *J. Biomed. Opt.* **22**(8), 086001 (2017).
162. A.-F. Swager et al., "Computer-aided detection of early Barrett's neoplasia using volumetric laser endomicroscopy," *Gastrointest. Endoscopy* **86**(5), 839–846 (2017).

Biographies for the authors are not available.